REVIEW PAPER

The Unique Properties of Superconductivity in Cuprates

K. A. Müller

Abstract Copper oxides are the only materials that have transition temperatures, T_c, well above the boiling point of liquid nitrogen, with a maximum T_c^m of 162 K under pressure. Their structure is layered, with one to several CuO_2 planes, and upon hole doping, their transition temperature follows a dome-shaped curve with a maximum of T_c^m. In the underdoped regime, i.e., below T_c^m, a pseudogap $\Delta^* \propto T^*$ is found, with T^* always being larger than T_c, a property unique to the copper oxides. In the superconducting state, Cooper pairs (two holes with antiparallel spins) are formed that exhibit coherence lengths on the order of a lattice distance in the CuO_2 plane and one order of magnitude less perpendicular to it. Their macroscopic wave function is parallel to the CuO_2 plane near 100 % d at their surface, but only 75 % d and 25 % s in the bulk, and near 100 % s perpendicular to the plane in yttrium barium copper oxide (YBCO) [1]. There are two gaps with the same T_c [2]. As function of doping, the oxygen isotope effect is novel and can be quantitatively accounted for by a vibronic theory or by the presence of bipolarons [2, 3]. These cuprates are intrinsically heterogeneous in a dynamic way. In terms of quasiparticles, bipolarons are present at low doping and aggregate upon cooling [2] so that probably ramified clusters and/or stripes are formed, leading over to a more Fermi liquid-type behavior at large carrier concentrations.

Keywords Superconductivity · Cuprates

K. A. Müller (✉)
Physik-Institut der Universität Zürich, CH-8057 Zürich, Switzerland
e-mail: irmamf@bluewin.ch

1 Scope of the Article

Since the discovery of superconductivity in hole-doped La_2CuO_4 [4, 5], a vast effort devoted to discovering new copper oxides with elevated superconducting transition temperatures, T_c, and to their understanding has appeared in the literature. All copper oxide-based superconductors contain CuO_2 layers. Their inherent properties are the existence of singlet Cooper pairs, a very small coherence length, and a unique phase diagram. More than 25 years after their discovery, the search for the origin of the unexpectedly high transition temperatures that most of them exhibit is regarded by the scientific community to be one of the truly challenging problems in condensed matter physics. The superconducting copper oxides are at present the only material class that exhibits superconductivity well above the boiling temperature of liquid nitrogen. As such, they can indeed be named high-temperature superconductors (HTSs).
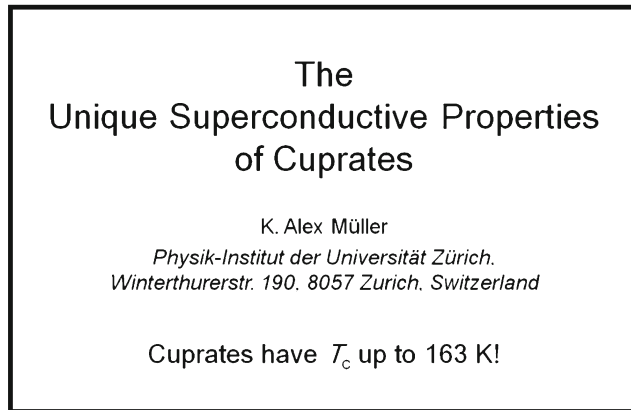
Over the past 3 years, the author has been invited to several conferences, including three major ones, to describe his understanding of the occurrence of superconductivity in the cuprates. The first was the APS March Meeting in Dallas in 2011 [6] on the occasion of the centenary of the discovery of superconductivity in Leyden, The Netherlands, and conjointly, the 25th anniversary of the one in the cuprates in Rüschlikon, Switzerland [4, 5]. Then a symposium at the University of Twente followed in September 2011 [7]. The next was the ICSM in Istanbul in the spring of 2012 [8] and, in the same year, the M2S in Washington in July [9].

The content and, therefore, their abstracts were closely the same. Above, I have reproduced a "unified" version. It

can also be taken as a summary of the content of the present paper, which reproduces most of the panels shown at these conferences together with my comments and explanations.

2 Description of and Comments to the Panels

Panel 1

The
Unique Superconductive Properties
of Cuprates

K. Alex Müller

*Physik-Institut der Universität Zürich.
Winterthurerstr. 190. 8057 Zurich. Switzerland*

Cuprates have T_c up to 163 K!

Panel 1 is the start panel, in which sometimes the word "unique" was replaced by "exceptional." In Houston, superconductivity up to 163 K was reached in one compound under pressure [10]. Other compounds barely made it to the temperature of liquid nitrogen
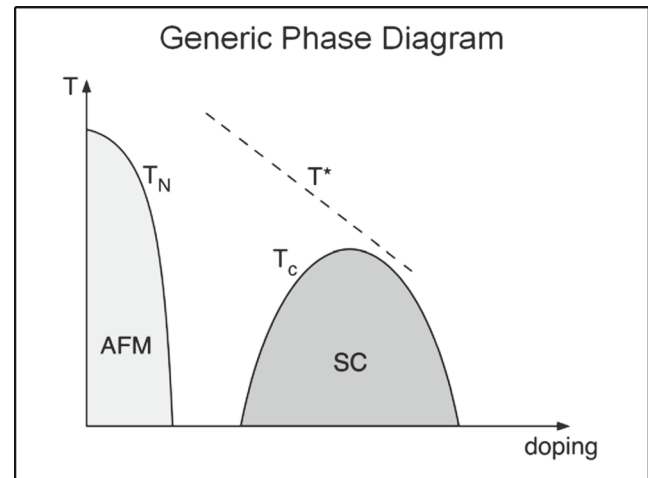
Panel 2

The Structure of Cuprates
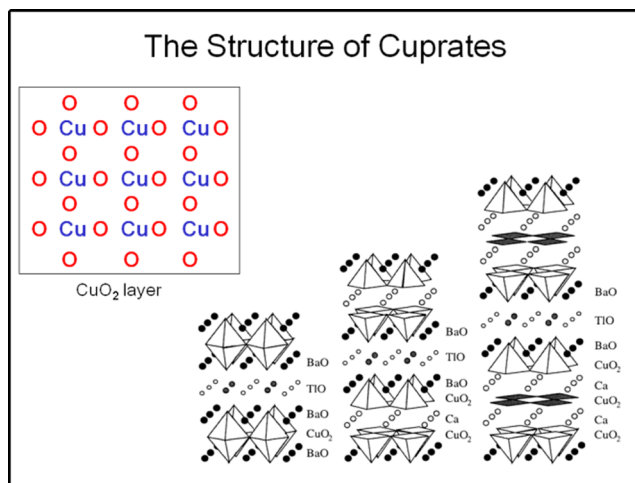
Here, the main structure found for all superconducting cuprates is shown. It contains CuO_2 *layers* with a structure found in perovskites, but there in three directions. The CuO_2 layers can be present once, twice, thrice, and also four times

in the unit cell. When undoped, these copper oxides are insulators and antiferromagnets because of the magnetic Cu^{2+} ions present.

Panel 3

Generic Phase Diagram

Upon hole doping, a generic phase diagram is found for all the cuprates investigated. It is shown schematically in this panel. At approximately 6 % of doping, superconductivity appears and T_c follows a dome-shaped curve with a maximum of T_c^m. In the underdoped regime, i.e., below T_c^m, a so-called pseudogap $\Delta^* \propto T^*$ is found. As a function of doping, T^* becomes smaller in a nearly linear way, but *never intersects* the T_c curve—a property unique to the copper oxides.

Panel 4
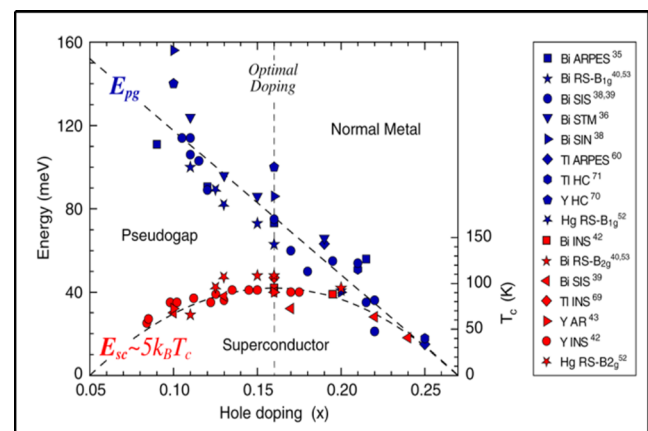
This panel reproduces data from many systems showing the progression of T^* and T_c, where the former curve

approaches the latter tangentially above optimum doping. This excludes all magnetism-based theories, which yield a quantum critical point at $T = 0$ near optimum doping, because the $T*$ line would have to intersect the one of T_c near this doping level. This was first found by Deutscher [11], based on Andreev reflections and now confirmed by many other data; see entries on the right of the panel (reprinted from [12]).

Panel 5
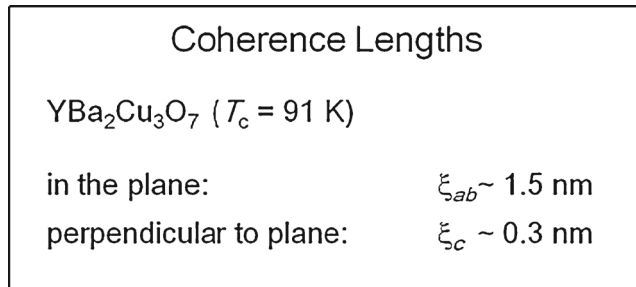
In all superconductors, Cooper pairs are present. They consist of two charge carriers with opposite spins which are coupled over a certain coherence length. Because of the high Fermi energy, their coherence lengths in metallic superconductors are up to several hundreds of angstroms. However, as shown in the panel, in the cuprates, they are only one to two lattice distances, and only a fraction of the unit cell distance along the c-axis [2]! We will see later that also the symmetry of the wave function in that direction is very different from that in the CuO_2 plane.
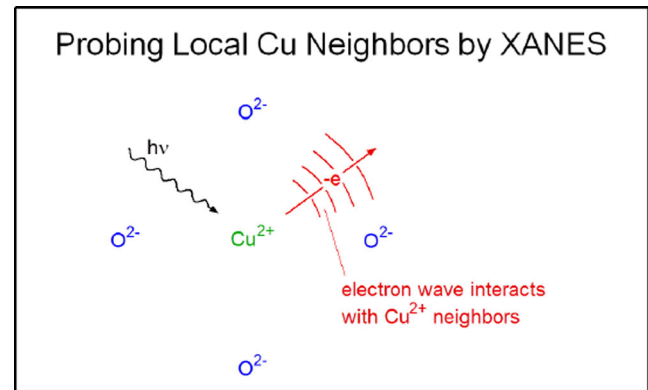
Panel 6
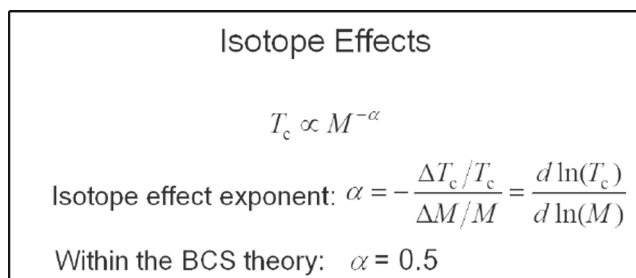
In the classical superconductors, the isotope effect was substantial in pointing to and supporting the Bardeen–Cooper–Schrieffer (BCS) theory. The key point is summarized in this panel: T_c is proportional to the mass of an elemental superconductor to an exponent α, which is 0.5 as predicted by BCS and observed in most of the cases.

In cuprates, very large isotope effects on $T*$ have been reported in two entirely different types of experiments: first, via X-ray absorption near-edge structure (XANES), and then with inelastic neutron experiments. We start with the former.

Panel 7

In XANES, high-energy photons impinging on the sample eject, here from a Cu^{2+} ion, an electron of given energy that interacts with its corresponding de Broglie wavelength with its neighbor ions.

Panel 8
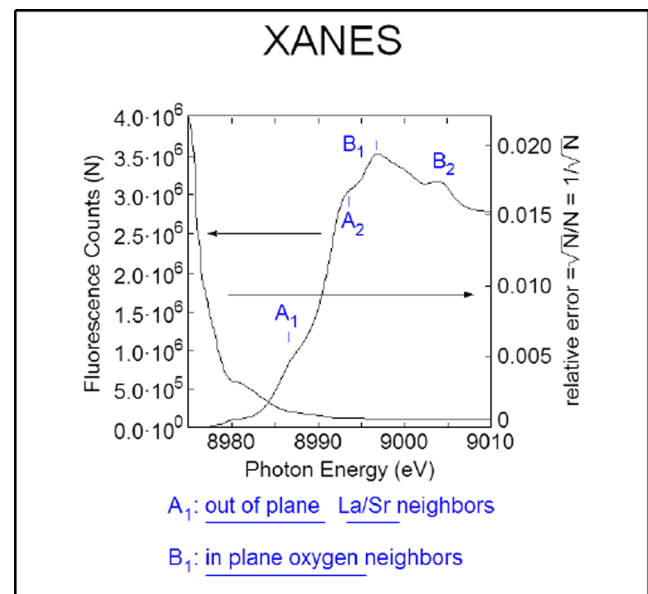
The resulting fluorescence in the experiment is plotted as a function of the impinging photon energy. An edge is

observed that depends on the neighbors either out of plane, A_1 and A_2, or in plane, B_1 and B_2. One can therefore monitor the change in the Cu^{2+} local neighbor distance either in or out of plane in an extremely short time (adapted from [13]).

Panel 9

The Stripe Formation Temperature T*

$$R = \frac{B_1 - A_1}{B_1 + A_1}$$
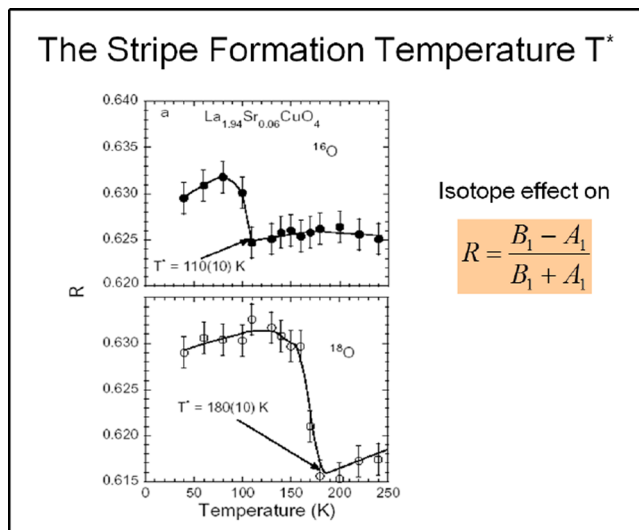
Upon replacing ^{16}O by ^{18}O, the ratio R is sensitive to the Cu^{2+}–O distance, as shown. As a function of temperature, a very large shift of 70 K in the detected step is recorded. Thus at T^*, a substantial change in the dynamics of the planar ligand–oxygen distance must be present. This is in clear contradiction to the theories advanced that propose an electronic origin of HTS, and ignored by that community to this day (reprinted from [13]).

Panel 10

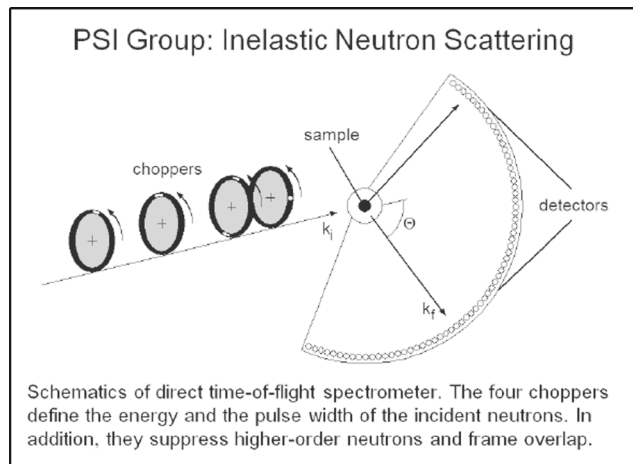The Very Large Oxygen Isotope Dependence on the Stripe-Formation Temperature T^*

Inelastic Neutron Scattering in YBCO 1248

A collaboration of

Paul Scherrer Institute:	D. Rubio Temprano, A. Furrer, K. Conder, J. Mesot
Institute Laue-Langevin:	H. Mutka
University of Zurich:	K. Alex Müller

To confirm the very large oxygen isotope effect found with XANES on T^*, an entirely different experiment that is sensitive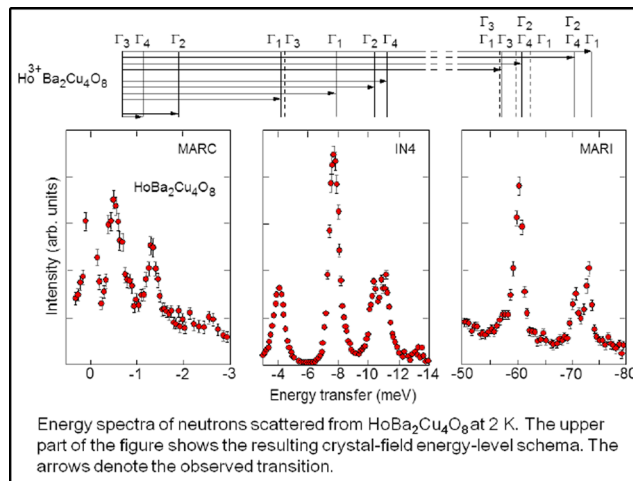 to the Cu^{2+}–O ligand distance was carried out by means of inelastic neutron scattering in Würenlingen, Switzerland.

Panel 11

PSI Group: Inelastic Neutron Scattering

Schematics of direct time-of-flight spectrometer. The four choppers define the energy and the pulse width of the incident neutrons. In addition, they suppress higher-order neutrons and frame overlap.

A beam of neutrons with defined energy and width impinges on the sample, where it is scattered and detected as a function of its wave vector, i.e., the scattering angle, by a circle of aligned detectors.

Panel 12

Energy spectra of neutrons scattered from $HoBa_2Cu_4O_8$ at 2 K. The upper part of the figure shows the resulting crystal-field energy-level schema. The arrows denote the observed transition.

Here, scattering data for HBCO 1248 are shown. This is a stoichiometric, lightly underdoped compound chosen to obviate questions regarding possible structural phase transitions (SPTs) or inhomogeneity. Indicated are the measured and the assigned crystal field transitions of Ho^{3+} replacing the rare-earth ion Y^{3+} (adapted from [14]).

Panel 13
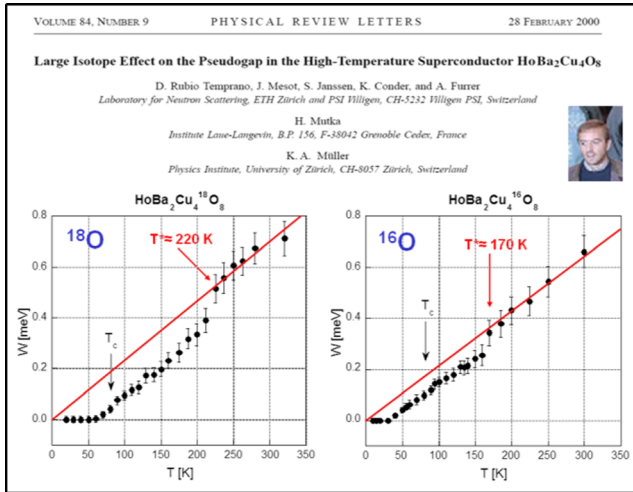
Shown is the ground state to the first excited Γ_4 state as a function of temperature of this transition. It is proportional to the A_2^2 crystal field. At $T*$, a jump occurs with a ^{16}O to ^{18}O isotope shift of 50 K comparable to that observed in lanthanum strontium copper oxide (LSCO) with XANES [14]. Also shown is a picture of D. Rubio Temprano, whose thesis work was under the direction of Prof. Albert Furrer at the ETH Zurich.

Panel 14
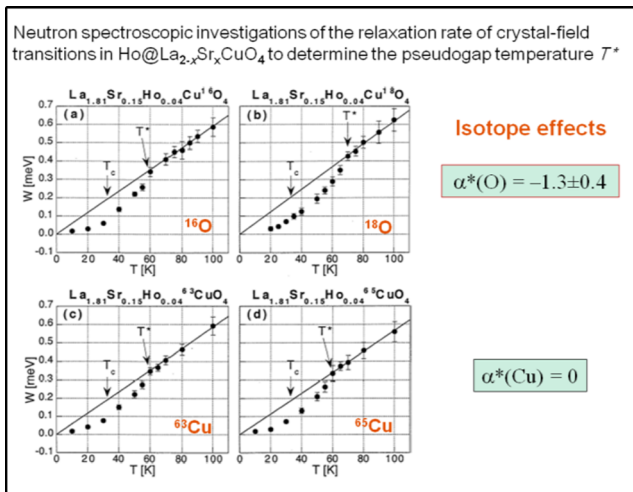
To further substantiate the enormous oxygen isotope shift at $T*$, experiments in LSCO were carried out in which the La^{3+} was substituted in part by Ho^{3+}, whose Γ_1 to Γ_4 transition was recorded for both ^{16}O to ^{18}O and ^{63}Cu to ^{65}Cu substitutions. Whereas for the former, an isotope shift of 10 K occurs, there is none for the latter. The reason is that in LSCO, the nearest neighbors to Cu^{2+} are oxygen ions on octahedral lattice sites. There exists an inversion

symmetry in their motion that is not crystal field active. In contrast, in YBCO, an isotope shift is observed for ^{63}Cu to ^{65}Cu substitution as expected because here the nearest neighbors to Cu^{2+} are located on a pyramid and the copper lacks inversion symmetry (the so-called Röhler mode is active). Note also that the isotope effect is large and negative (from [15]).

Panel 15

Very Large Oxygen Isotope Effects

– XANES (A. Lanzara *et al.*)
– Inelastic Neutron Scattering (A. Furrer group)
– μ-ion Rotation (H. Keller *et al.*)

All eight types of experiments are well accounted for by the

– intersite JT bipolaron theory (V. Kabanov & D. Mihailovic)
– two component-band theory (A. Bussmann-Holder & H. Keller)

Here is a summary of the isotope effects on $T*$ discussed so far and the theories that account for them. Before we go on to these effects observed on T_c, we summarize the relevant vibronic theory.

Panel 16

Vibronic Theory

$$H = H_1 + H_2 + H_{e-l} + H_l, \qquad H_l = \hbar\omega\sum_i b_i^+ b_i$$

$$H_1 = H_{tJ}(d)$$

$$H_2 = H(p)$$

$$H_{e-l} = -\gamma\sum_{i,\sigma}[x_i n_{ip} + x_j n_{jd}] - \tilde{\gamma}\sum_{i,j}x_i(d_i^+ p_j + H.c.)$$

Polaron binding energy $E_b = \gamma^2/2M\omega^2$

The Hamiltonian consists of four terms. The first encompasses the electronic d functions of the Cu^{2+} ions present, found in the $t-J$ model. The second is due to the oxygen p band. The third is the vibronic interaction between the two bands: in it, the first term is the linear interaction between the electronic densities and the respective ionic displacements, and the second term is the exchange between the two bands. The latter is responsible for only one transition temperature and not for two, as predicted by the author
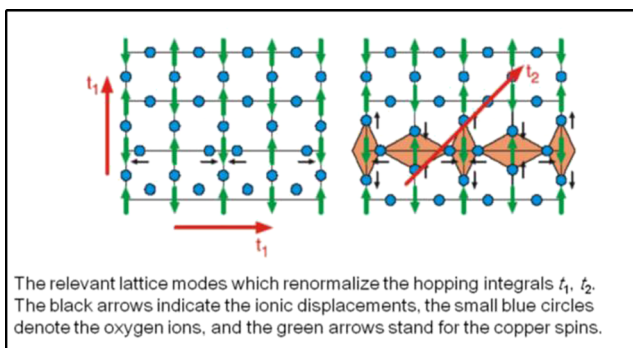
almost two decades ago [16]. The last term describes the usual lattice dynamics. This model yields polarons with the binding energy amount shown. They are proportional to the square of the interaction constant γ and inversely proportional to the ionic mass and the phonon frequency. See [17].

Panel 17
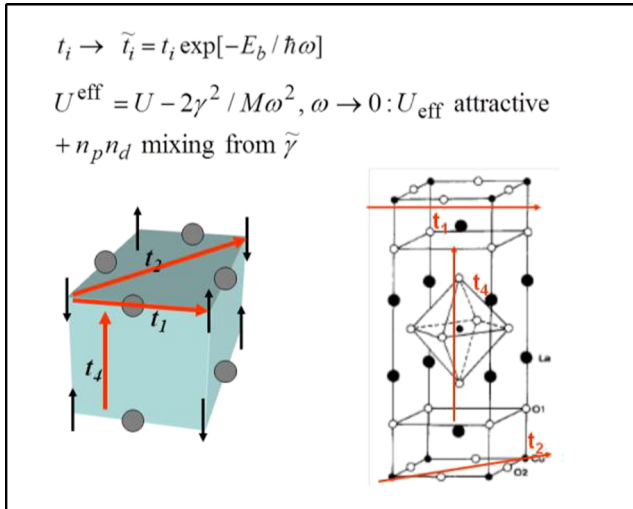
Very important is (i) that the tunneling t in the t–J model gets renormalized exponentially, as shown, and decreases when the polaron binding energy increases and (ii) that the electronic repulsion, i.e., the Hubbard U, between two polarons is reduced by four times the polaron binding energy, and this down to the point at which it can become negative, i.e., attractive. That means bipolarons become stable. Also shown are the possible four tunneling paths with their respective unrenormalized amounts, at the left with the nearest neighbors and at the right in the lattice unit cell [17].

Panel 18

The relevant lattice modes which renormalize the hopping integrals t_1, t_2. The black arrows indicate the ionic displacements, the small blue circles denote the oxygen ions, and the green arrows stand for the copper spins.

Here is the situation for a CuO_2 layer, with the hopping terms t_1 and t_2 and the corresponding lattice modes (reprinted from [17]).

Panel 19
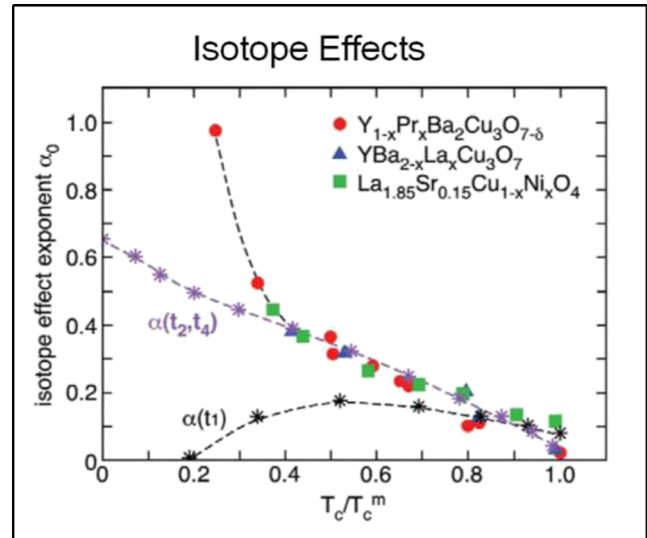
This panel shows the isotope effects measured for three compounds as a function of reduced transition temperatures $t = T_c/T_c^m$ below maximum as well as those computed from the vibronic theory for hopping t_1, t_2, and t_4. Whereas the progression with the former does not follow the experiments, the one for the latter does so quantitatively from $t = 1$ to 0.4. Here, it should be noted that the lattice deformation coupling with t_2 is the one of the Jahn–Teller effect. Below 0.4, the observed isotope shifts are much larger than the computed ones. We ascribe this deviation to the mean field computation of the theory, which does not reflect the granularity present for underdoping well. See [18], adapted from [17].

Panel 20

$$\alpha(n, T_c) = \gamma(n)\frac{n}{T_c(n)}\frac{\partial T_c(n)}{\partial n}$$
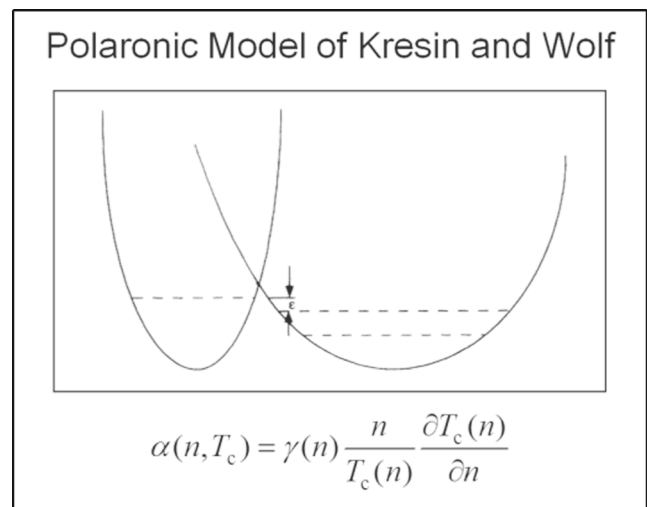
Therefore, I expected that a theory by Kresin and Wolf, published in 1994, might describe the situation better. In it, polarons oriented along the c-axis, as shown, were assumed.

However, the derivation would also hold if the polarons, or better bipolarons, lie in the CuO_2 layer. The relatively simple formula for the isotope exponent is included in the panel as well. Note that α is proportional to the derivative of the carrier concentration n. It therefore reflects the sign inversion of α observed for T^* and T_c (reprinted from [19a], see also [19b]) .

Panel 21
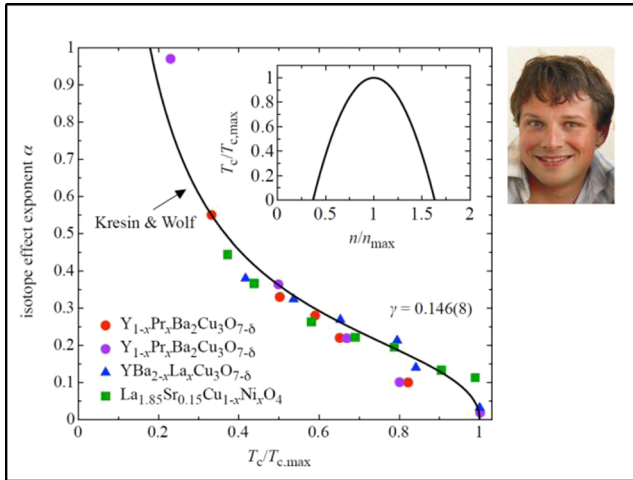
Here is the outcome of using the Kresin–Wolf formula with the measured isotope effects for $T_c/T_c^m \leq 1$ down to the superconductor–isolator transition, T_{S-I}. This was computed by using the T_c domes published. The agreement is really spectacular, about as good as that of the critical behavior of the order parameters in structural phase transitions measured by the author's group at the time and that of the renormalization group theory. Note that it holds down nearly to T_{S-I}, where $\alpha \approx 1$, i.e., twice as large as in BCS theory. From this agreement, we conclude that the Kresin–Wolf formula holds also for in-plane polarons and, in fact, proves their existence. I also show the picture of Dr. Stephan Weyeneth, with whom these results were obtained (reprinted from [20]).

Panel 22

The isotope experiments and the agreement with the Kresin–Wolf formula lead to the question whether there

are data that support this result. First, let us consider the ground state of a single polaron. Because of the coupling of the charge with the lattice, the product of a nuclear and an electronic wave function is present. Therefore, the nuclear and electronic degrees of freedom *cannot be separated*, as is the case in the Born–Oppenheimer approximation generally used, where only a single nuclear/electronic term is present, and the respective energies and masses are very different.

Panel 23
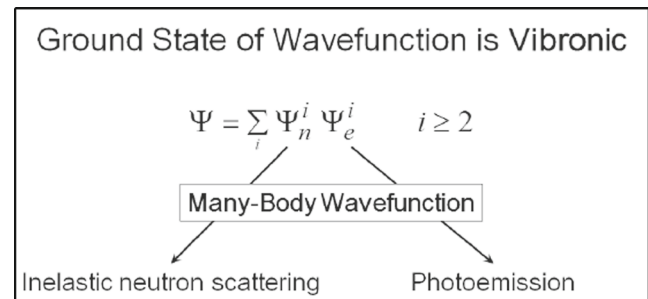
Of course here, we are dealing with multiparticle wave functions as shown schematically. This can be probed experimentally with inelastic neutron scattering for the lattice dynamics and with photoemission for the electronic part. As will be shown in the next two panels, in both experiments, an anomaly is present near energies of $\approx$70 meV as a function of the wavelength, pointing to the vibronic character of the HTS cuprates. This was pointed out by the author well over a decade ago [2].
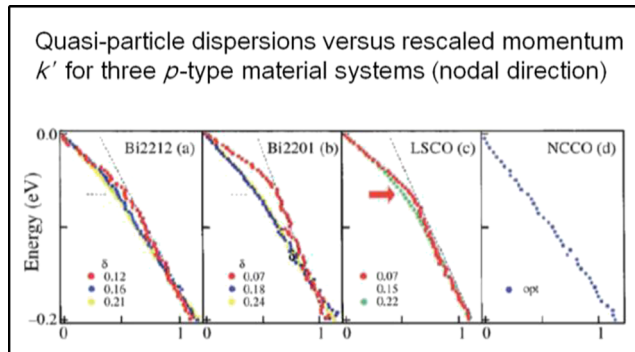
Panel 24
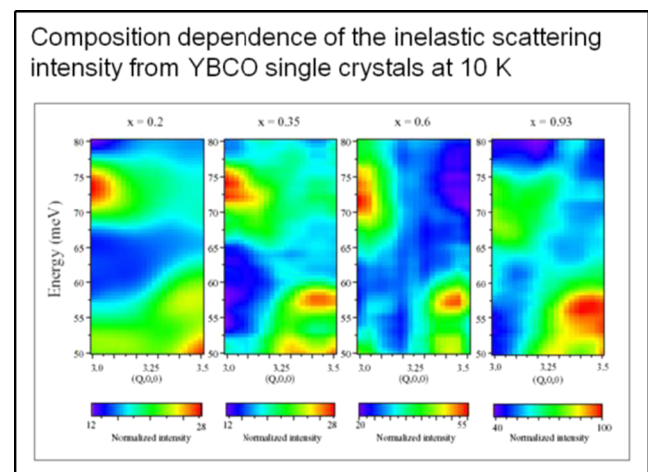
Here are the inelastic neutron scattering data of Egami's group along the [Q,0,0] direction for four different hole
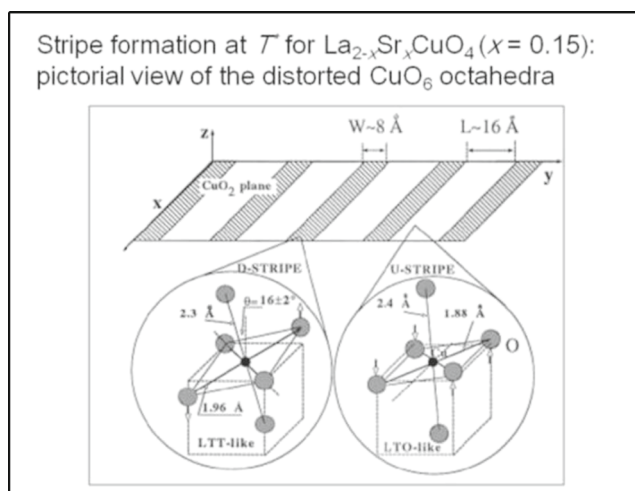
dopings in YBCO. For $x = 0.35$, in the middle of the zone, a discontinuity of a strong excitation between 55 and 73 meV is seen, confirming earlier results by Pintchovius and Reichart [21]. See [22], reprinted from [23].

Panel 25

Quasi-particle dispersions versus rescaled momentum k' for three p-type material systems (nodal direction)

In this panel, photoemission data of Lanzara et al. are shown for four superconductors along the 0 to 1 direction. For the three with hole doping, a clear knee in the linear dispersions occurs near 70 meV. In the electron-doped one, this kink is not present. The two experiments shown reflect the lattice dynamic and the electronic excitations due to the polarons present [24].

Panel 26

Stripe formation at T' for $La_{2-x}Sr_xCuO_4$ ($x = 0.15$): pictorial view of the distorted CuO_6 octahedra

The existence of two conformations of nearest neighbors to the Cu^{2+} ions in LSCO was actually shown in the group of Bianconi in Rome quite early on by X-rays, and commented on by Mihailovic and Müller [25], along with confirming experiments such as NMR, Mössbauer effects,

and optical reflection data. One of the two conformations is a nearly regular octahedron. The other consists of two oxygen ions that moved symmetrically toward the Cu^{2+} and two that moved outward, all four near the CuO_2 plane. This is clearly the Q_2 Jahn–Teller-active conformation. Note that because of the two oxygen ions that have moved outward, the oxygen–oxygen distance is larger than the one imposed by the lattice, and therefore, the octahedron in question gets tilted by about 6° away from the c-axis direction (reprinted from [26]).

Panel 27

The discovery of LSCO was based on the Jahn-Teller polaron concept.

In the past few years, the simultaneous presence of Jahn-Teller bipolarons and Fermions has been documented quite well, based on a two quasi-particle scenario.

In the upper part of panel 26, the Rome interpretation in terms of so-called stripes was shown. The white stripes are undistorted octahedral conformations. I view them as metal-like conducting, i.e., delocalized holes, and therefore not Jahn–Teller active, whereas the others with trapped holes are Jahn–Teller (JT) active.

We now come to the central part of the description of the hole-doped copper oxides.

Panel 28

From single to bi-polarons with Jahn-Teller character and metallic cluster stripes in hole-doped cuprates

K.A. Müller

University of Zürich
Winterthurerstr. 190, 8057 Zürich
Switzerland

When discussing panel 17, it was pointed out that the effective repulsion U can become negative, i.e., attractive, so that bipolarons can form at T^*. In agreement with this assignment, very large oxygen isotope effects were found by EXAFS (see panel 9) and inelastic scattering (panel 12). This was first proposed by the author in a review article in 2007 [27].

Panel 29

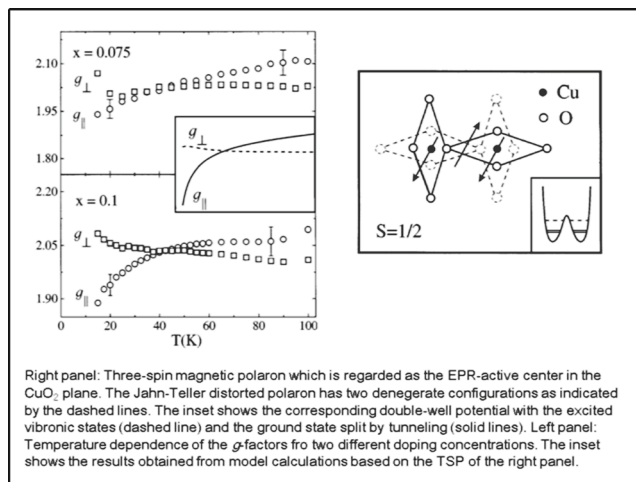Experiments in support of this scenario are

momentum-space dependent:
– Photoemission (A. Lanzara *et al.*)
– Inelastic neutron scattering (T. Egami *et al.*)

real-space dependent:
– EXAFS (A. Bianconi *et al.*)
– EPR (B. Kochelaev, A . Shengelaya)
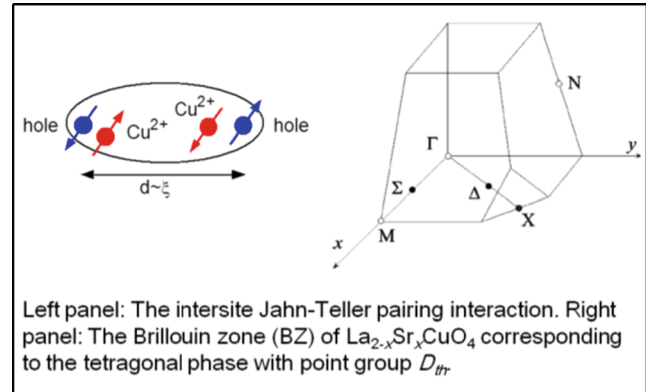– PdF's (S. Billinge *et al.*)

Here, we recall the already reviewed photoemission and inelastic neutron scattering work, i.e., wave vector-dependent data, and then that reflecting real space. With that, the determination of the structure of the bipolaron became possible, first by an analysis of the three-spin polaron observed by electron paramagnetic resonance (EPR), the lattice deformation determined by inelastic neutron scattering, and the already discussed local lattice deformation of Bianconi's group.

Panel 30

Right panel: Three-spin magnetic polaron which is regarded as the EPR-active center in the CuO_2 plane. The Jahn-Teller distorted polaron has two denegerate configurations as indicated by the dashed lines. The inset shows the corresponding double-well potential with the excited vibronic states (dashed line) and the ground state split by tunneling (solid lines). Left panel: Temperature dependence of the g-factors fro two different doping concentrations. The inset shows the results obtained from model calculations based on the TSP of the right panel.
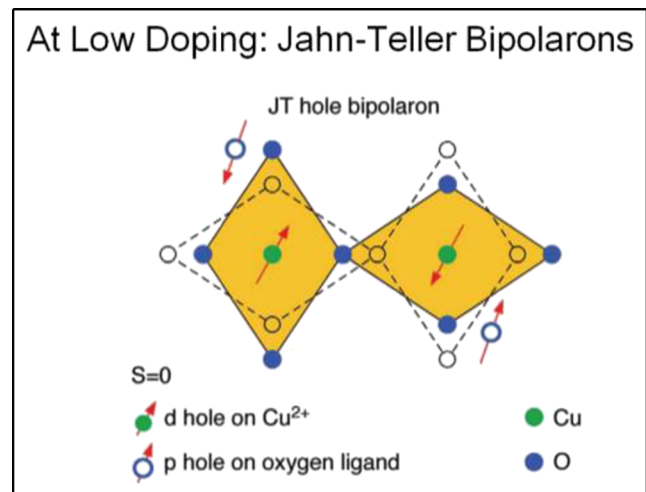
The three-spin center in LSCO was discovered by J. Sichelschmidt in Elschner's group in Darmstadt. It is a center with spin $S = 1/2$, axial along the c-axis detected by EPR. The remarkable property is that its gyromagnetic values $g_\perp$ and $g_\parallel$ *cross as a function of temperature*, and this for two different dopings. The two conformations which tunnel between each other are the planar JT ones. This center was proposed earlier by Emery and Reiter [28] and has a higher energy than the bipolaron carrying two carriers because of the ensuing oxygen lattice deformations. Therefore, the three-spin polaron is very likely trapped at a positive lattice defect, i.e., a substitutional Sr^{2+} for Al^{3+}. To confirm this, an ENDOR experiment would have been appropriate (reprinted from [29]).

Panel 31

Left panel: The intersite Jahn-Teller pairing interaction. Right panel: The Brillouin zone (BZ) of $La_{2-x}Sr_xCuO_4$ corresponding to the tetragonal phase with point group D_{ttr}.

Here schematically, the trapping of the second carrier is shown to form a bipolaron. It is in principle equivalent to the effective negative U center of Anderson [30]. With his note, Anderson solved the problem of doped inhomogeneous semiconductors in which neither conductivity nor spin resonance was detected because he showed that due to the local lattice deformation, two trapped carriers with antiparallel spin, i.e., $S = 0$, had a lower energy than a single trapped carrier with spin. The right panel is from [31].

Panel 32

At Low Doping: Jahn-Teller Bipolarons

JT hole bipolaron

$S=0$

d hole on Cu^{2+} Cu

p hole on oxygen ligand   O

Here is the bipolaron as proposed in 2000 by Kabanov and Mihailovic. Two holes with antiparallel spin are trapped on oxygen orbitals next to two two-valent copper ions with spin $S = 1/2$. The oxygens are displaced with local t_2 conformations as in the three-spin polaron. It is this Jahn–Teller deformation which makes the trapping of the two holes possible. The two copper spins are oriented antiparallel to each other and to the rest of the AFM lattice. As the bipolaron carries no spin, it can be mobile in the AFM lattice (adapted from [31, 32]).

Panel 33
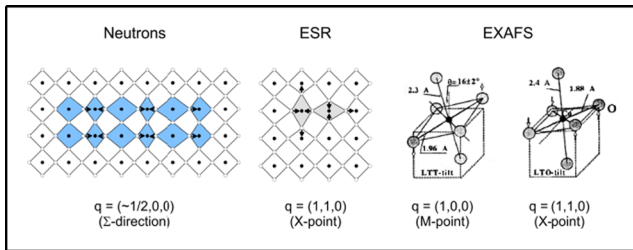
Kabanov and Mihailovic arrived at their model with the X-ray analysis of Bianconi et al. shown in panel 26, the three-spin polaron from EPR, panel 30, and the lattice deformation obtained by inelastic neutron scattering of Egami's group, panel 24. All three are summarized in this panel. The left panel is from [32], the center panel from [31], and the right panels (EXAFS) are from [33].

Panel 34
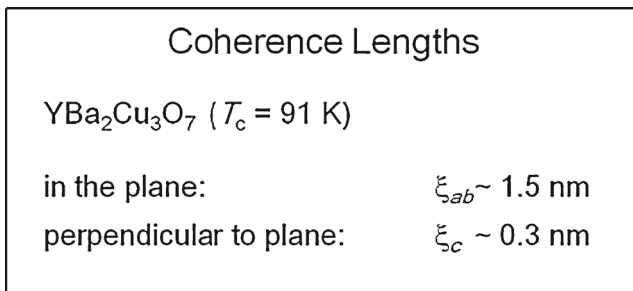
Before going on, we recall panel 5, in which the experimentally determined coherence length of the Cooper pairs was shown in the CuO$_2$ plane; it is close to the size of the bipolaron, and we can regard the Cooper pairs with their short coherence lengths in the cuprates as being formed by the bipolarons.

Panel 35
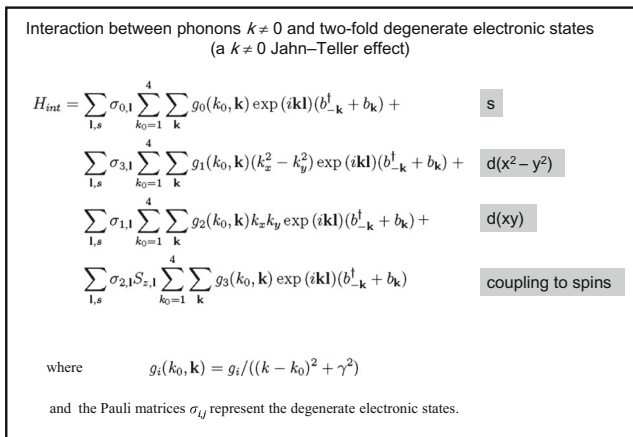
Here, the four possible interactions of finite wavelength phonons, $b_k^{+/-}$ with the doubly degenerate state of the

bipolaron using Pauli matrices are shown, as they appear in the paper of Kabanov and Mihailovic [31]. The first term is due to the breathing mode, the second and the third are the interactions with JT-active modes, and the fourth results from the magnetic interaction. The $g_i(k_0, k_i)$ are the wavelength-dependent interaction constants. The second and the third are the relevant ones.

Panel 36
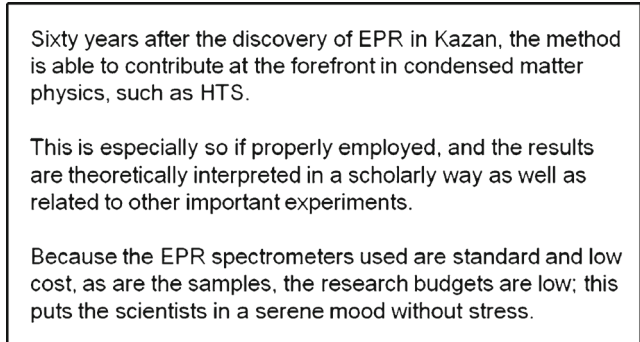
The behavior of the bipolarons and their formation energy could subsequently be investigated by EPR, and this panel recalls the advantages of this well-known method that provides information in real space as a function of time of the quasiparticles in question.

Panel 37
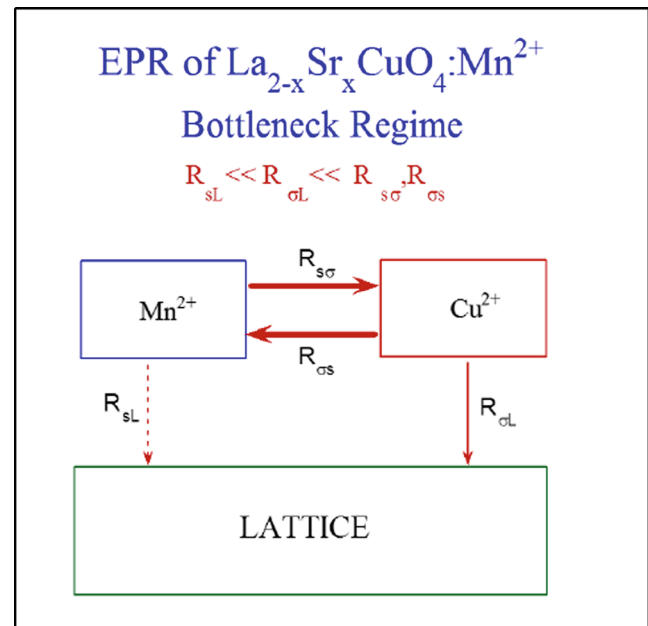
The way EPR was employed to obtain the desired information is shown in this panel. Mn^{2+} ions were substituted in small concentrations for the intrinsically present Cu^{2+}. The relaxation of the Mn^{2+} occurs mainly to Cu^{2+} in the lattice and not directly to the lattice vibrations. See [34].

Panel 38
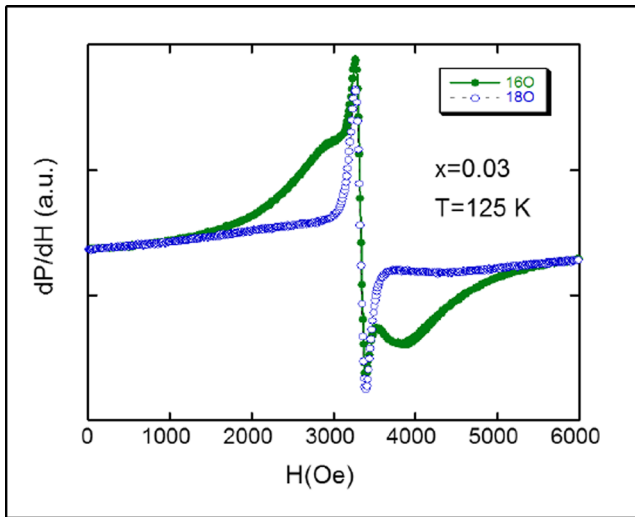
Here, the recorded EPR spectrum is shown. It consists of a broad and a narrow line very near the g value of the free spin of Mn^{2+}. The broad line shows an oxygen isotope effect and the narrow one does not. The former was assigned to the coupling and spin diffusion of the Cu^{2+} in the lattice, and the narrow one to Mn^{2+} ions in metallic clusters present. From the analysis of the broad EPR line, the relaxation of the Cu^{2+} to the lattice could be obtained. Because of the short time inferred, it could now be understood why no EPR from the Cu^{2+} has ever been observed: the line is too broad (reprinted from [35]).
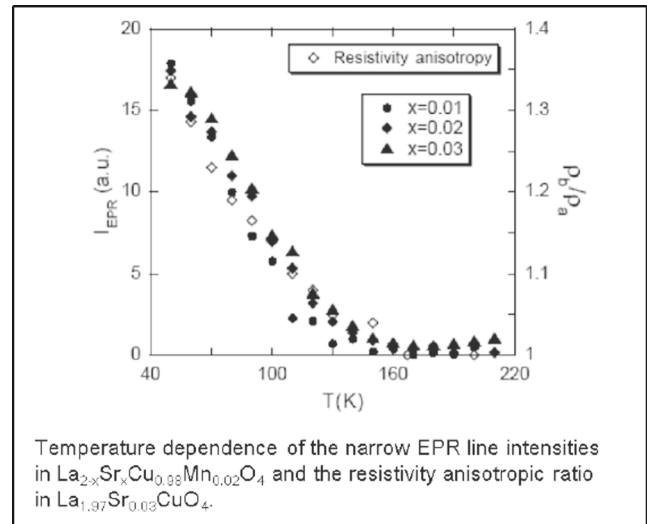
Panel 39
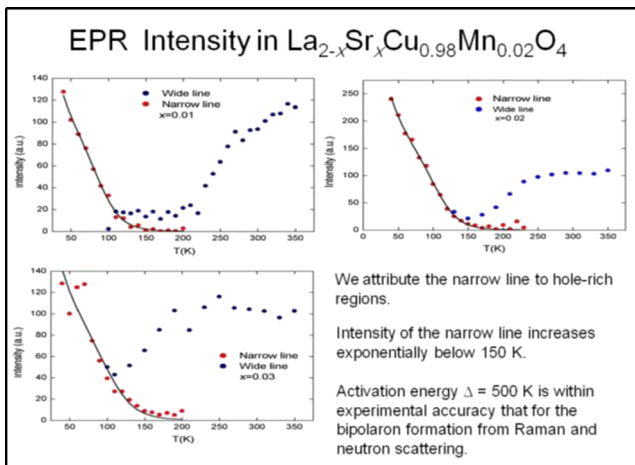
This panel shows the intensity of the broad and the narrow Mn^{2+} EPR lines as a function of temperature for 1, 2, and 3 % of Mn^{2+} doping. Upon cooling, the broad line intensity decreases substantially, whereas the narrow one increases exponentially. The activation energy is near 500 K, independent of the doping, and gives the formation energy of the bipolarons that cluster into metallic domains or stripes. This energy is in the range Kochelaev and Safina calculated from
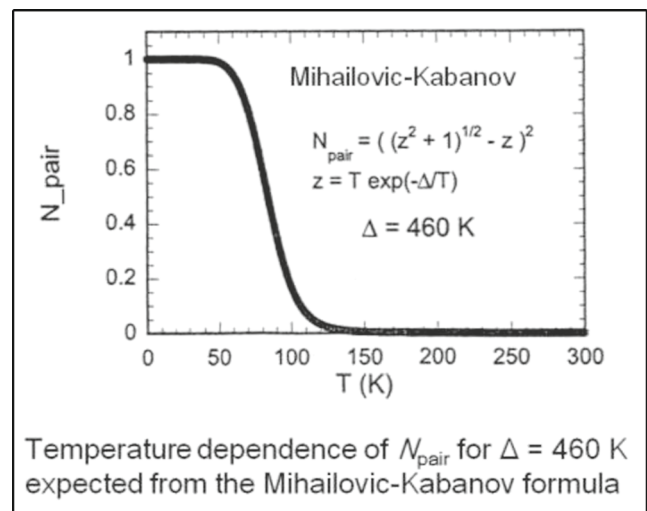
first principles to be between 100 and 700 K depending on the correlation energy of the two trapped holes present [35].

Panel 40

Temperature dependence of the narrow EPR line intensities in $La_{2-x}Sr_xCu_{0.98}Mn_{0.02}O_4$ and the resistivity anisotropic ratio in $La_{1.97}Sr_{0.03}CuO_4$.

This is a plot in which the Mn^{2+} EPR lines of the three doping concentrations of panel 39 are presented together with the resistivity anisotropy ratio in LSCO single crystals obtained by Ando et al. [36]. The latter macroscopic quantity grows exponentially as does the microscopic EPR. Ando et al. attributed this to the growth and alignment of the stripes present. This is in agreement with the behavior found microscopically with EPR. It should be noted that the hole concentration present in the LSCO is *under the 6 % needed for the occurrence of bulk superconductivity*. Therefore, in this case, the metallic stripes present are an intrinsic property of the hole-doped lattice as such (reprinted from [37]).
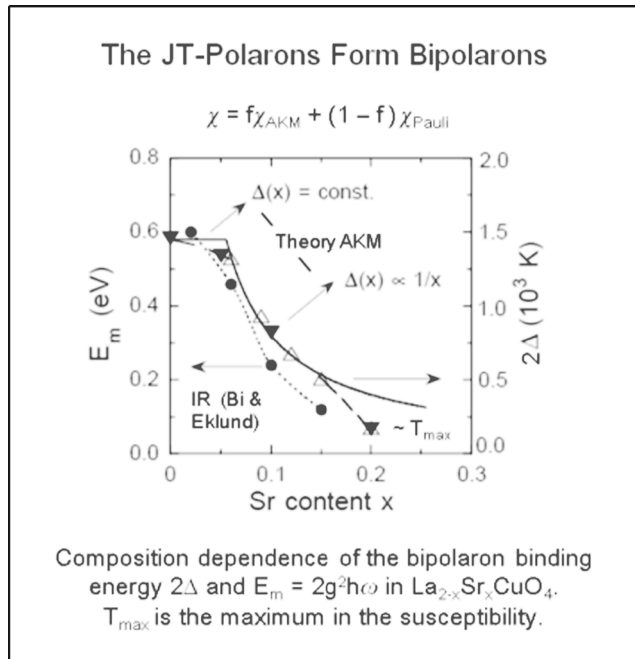
Panel 41

Temperature dependence of N_{pair} for $\Delta = 460$ K expected from the Mihailovic-Kabanov formula

For a doping n, there are only $N = n/2$ pairs possible upon cooling. Mihailovic and Kabanov provided the
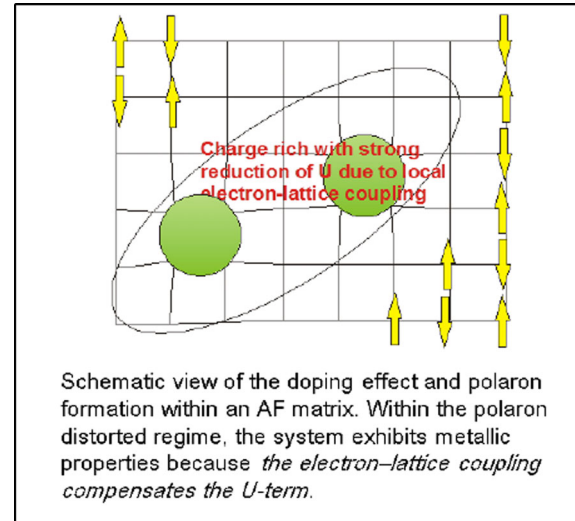
analytical expression for $N(T)$ in their paper quoted in panel 32. It is shown here for a given pairing energy Δ. Upon cooling, the number of bipolarons increases first exponentially.

Panel 42

The JT-Polarons Form Bipolarons

$$\chi = f\chi_{AKM} + (1-f)\chi_{Pauli}$$

Composition dependence of the bipolaron binding energy 2Δ and $E_m = 2g^2\hbar\omega$ in $La_{2-x}Sr_xCuO_4$. T_{max} is the maximum in the susceptibility.

This panel summarizes the binding energy $\Delta(x)$ for the bipolarons as a function of the hole doping x from three different efforts: (i) the theory of Alexandrov, Kabanov, and Mott (AKM) [38], (ii) the infrared (IR) data of Bi and Eklund [39], and (iii) the susceptibility χ data according to the theory of AKM plus a Pauli temperature-independent term. It should be noted that $\Delta(x)$ in the AKM theory is constant up to 5 %, which is in agreement with the doping-independent amount of $\Delta(x)$ up to 3 % with EPR shown in panels 39 and 40. Above 5 %, $\Delta(x)$ follows a dependence of $1/x$ approximately for the quite different type of IR and χ data. Near-optimum doping, deviations from theory and experiment occur because of bipolaron interactions (from [40]).

Panel 43

Schematic view of the doping effect and polaron formation within an AF matrix. Within the polaron distorted regime, the system exhibits metallic properties because *the electron–lattice coupling compensates the U-term.*

To understand the bipolaron interactions, we start with a schematic view of a single bipolaron and its interaction with the AFM lattice (as drawn with A. Bussmann-Holder).
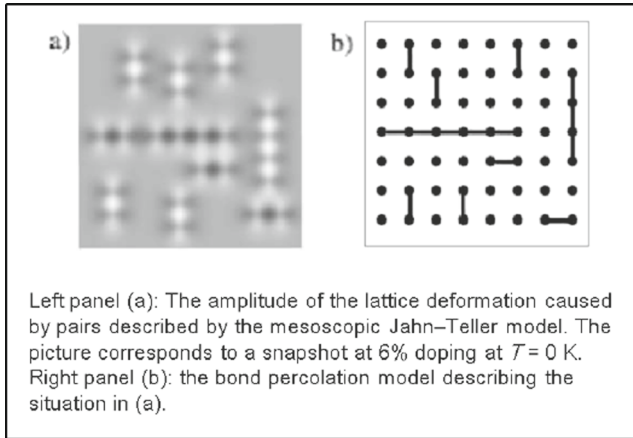
Panel 44

Polaron–Bipolaron Stripes
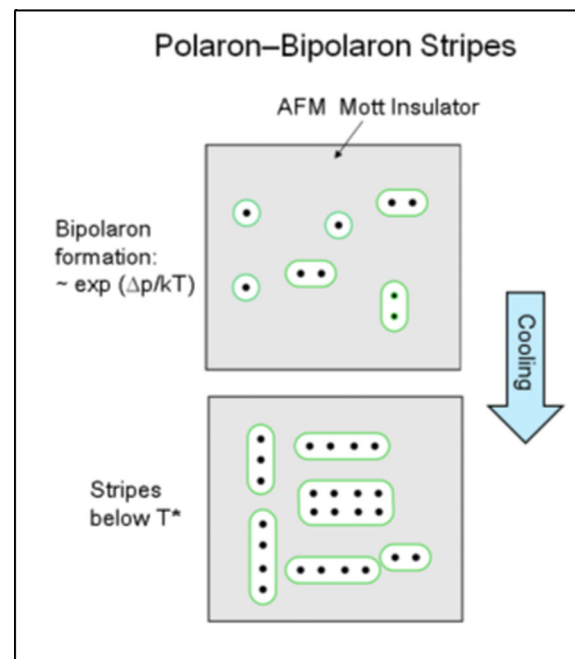
Based on panel 43, here is a schematic view of the cluster-ing of bipolarons into stripes. In this context, remember the

discussion on panel 40 with the same exponential temperature dependence of the narrow EPR line and Ando's resistivity anisotropy data in single-crystal low-doped LSCO.

Panel 45

Left panel (a): The amplitude of the lattice deformation caused by pairs described by the mesoscopic Jahn–Teller model. The picture corresponds to a snapshot at 6% doping at $T = 0$ K. Right panel (b): the bond percolation model describing the situation in (a).

On the left, the lattice deformation at 6 % doping in the CuO$_2$ plane for the *dynamic* mesoscopic Jahn–Teller model is shown and, on the right, the corresponding percolation model (reprinted from [41]).

Panel 46
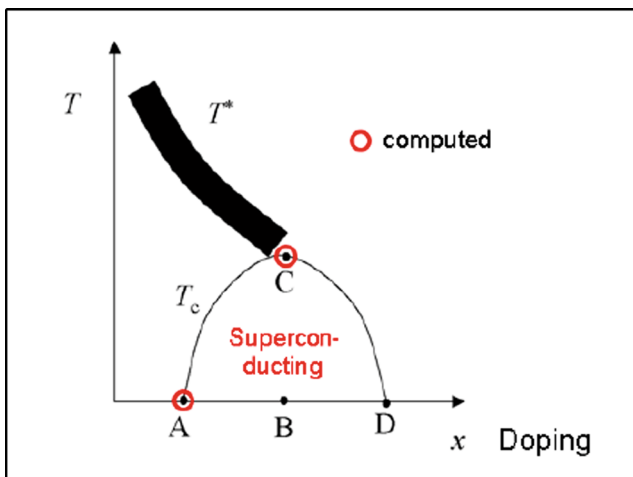
The x versus T phase diagram results from the mesoscopic model. The remarkable results were (i) an understanding of the minimum coherence length observed, (ii) the correct percentage of holes for which the onset of superconductivity is observed (6 %), and (iii) the correct percentage of holes ($\sim$15 %) to achieve the maximum value of T_c, i.e., T_c^m, and T_c^m itself (from [41]).

Panel 47

T. Mertelj, V. V. Kabanov and D. Mihailovic (2004)
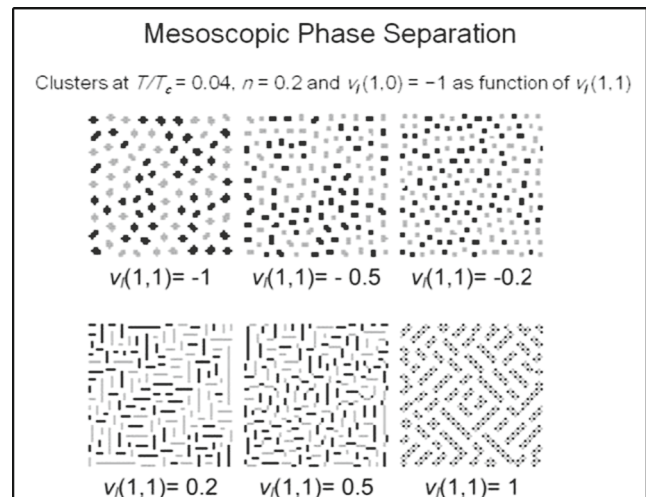*Josef Stefan Institute and University in Ljubljana*

Monte Carlo Simulation of $H = H_{JT} + V_{Coulomb} + H_{Strain}$

$$H_{strain} = g \sum_i S_i^* \varepsilon_i + \frac{1}{2}\left(A_1 e_{1,i}^2 + A_2 e_{1,i}^2 + A_3 e_{1,i}^2\right)$$

With Saint Venant's compatibility conditions, as applied to atomic lattices by A.R. Bishop, T. Lookman, A. Saxena and S.R. Shenoy.

The agreement between the mesoscopic model and the experimental results in panels 45 and 46 is remarkable, despite the fact that the percolative clustering and the stripe formation, observed especially by Tranquada's group [42], were not found. What is missing was recognized in Ljubljana to be the *strain interaction* between the bipolarons present. This panel summarizes this effort. The interaction term due to strain is shown. Note that the Saint-Venant compatibility condition is taken into account. In the latter, a divergence of a certain inelastic strain vector has to be zero, as discovered by Barré de Saint-Venant for the stability of railway bridges in the middle of the nineteenth century and rediscovered on the microscopic scale by Alan Bishop's group in Los Alamos for magnetic phases.

Panel 48

Mesoscopic Phase Separation

Clusters at $T/T_c = 0.04$, $n = 0.2$ and $v_l(1,0) = -1$ as function of $v_l(1,1)$

$v_l(1,1)= -1$ $v_l(1,1)= -0.5$ $v_l(1,1)= -0.2$

$v_l(1,1)= 0.2$ $v_l(1,1)= 0.5$ $v_l(1,1)= 1$

Here are snapshots of simulations discussed in panel 47 for $t = 0.04$, $n = 0.2$, and $v_l(1,0)$, as a function of $v_l(1,1)$, where t is the reduced temperature (T/T_c), n is the density, and $v_l(1,0)$ and $v_l(1,1)$ stand for the short-range nearest and next-nearest neighbor interactions [43]. Clearly visible

is the formation of stripes, which depending on the interaction of $v_l(1,1)$, are aligned along {1, 0} or {1, 1} in the plane (reprinted from [44]).

Panel 49
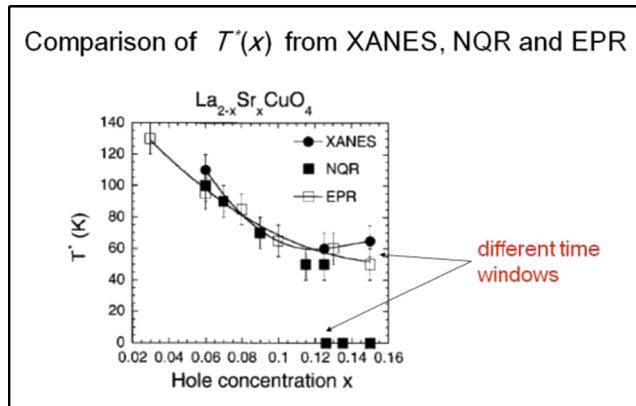
In the work shown so far, no allusion has been made regarding the dynamics present, say, the stripe generation movement and annihilation occurring in the AFM insulating matrix. This may be estimated from the observation of the generation of stripes or clusters below the onset at T^* as a function of temperature. Shown are the results from XANES, EPR, and NMR. Of these, the observation time is the shortest in XANES, namely $\approx 10^{-13}$ s (X-rays), whereas in EPR, it is 10^{-10} s, and in NMR, 10^{-7} s. One recognizes that the three yield the same $T^*(x)$ dependence up to optimum doping at $x = 0.13$, but there T^* drops to zero. For NMR, this occurs because the stripes' dynamics is faster than the time over which NMR, but not EPR and XANES, is observed (drawn by A. Shengelaya).
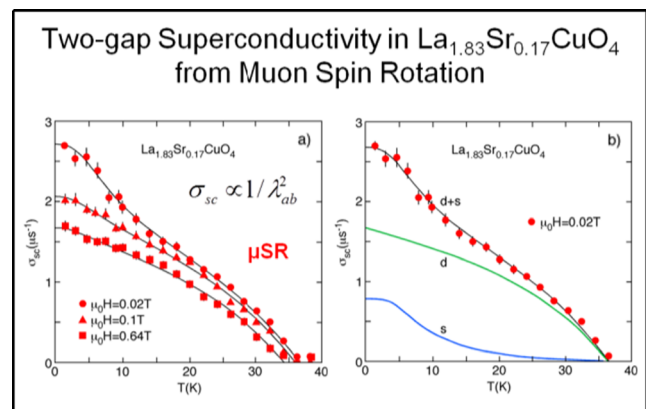
Panel 50
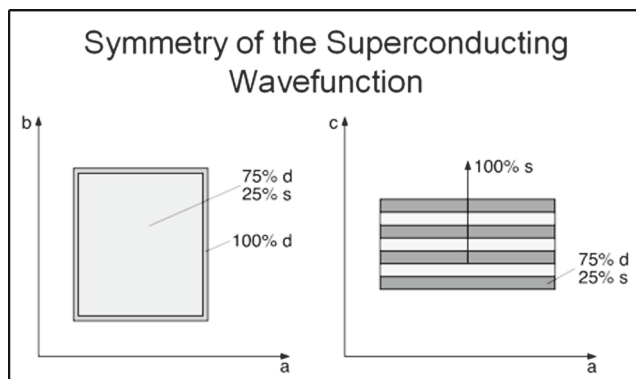
Single-band theories, such as the $t–J$ model, propose a pure d symmetry for the macroscopic wave function in

the cuprates. This is indeed observed with surface-sensitive experiments such as SQUIDS or the often quoted tricrystal experiment of Tsuei and Kirtley [45]. However, from the existing data, the author proposed, already back in 1995, that the wave function contains a d and an s component, but only one transition T_c, with the two symmetries stemming from two electronic bands. As commented in panel 16, the reason for this is the exchange between the two.

This panel actually summarizes the observations that will be shown in more detail in the next panels: in the CuO_2 plane at the surface, 100 % d, inside 75 % d, and 25 % s, in agreement with the group theoretical analysis of Iachello [46], and surprisingly, 100 % s along the tetragonal c-axis. The latter property could be derived from the vibronic theory discussed in panel 16.

Panel 51

There are a number of experiments confirming the picture shown in panel 50; see [47]. For clarity and brevity, we show the data obtained at the Swiss Muon Source at the PSI in Würenlingen by Khasanov et al. Muon rotation is a local probe so that the muons, depending on their energy, stop near the surface or in the bulk and thus are ideally suited for investigating the wave function as a function of the distance from the surface. The relaxation rate $\sigma_{sc}(T)$ is inversely proportional to the square of the London penetration depth $\lambda(T)$. At low magnetic field, the two s and d components are clearly visible, but less so at higher magnetic fields. This is due to the presence of more vortices with their surface and, therefore, d character [47]. On the left, the decomposition of $\sigma_{sc}(T)$ into the two components is shown. (Reprinted from [48]).
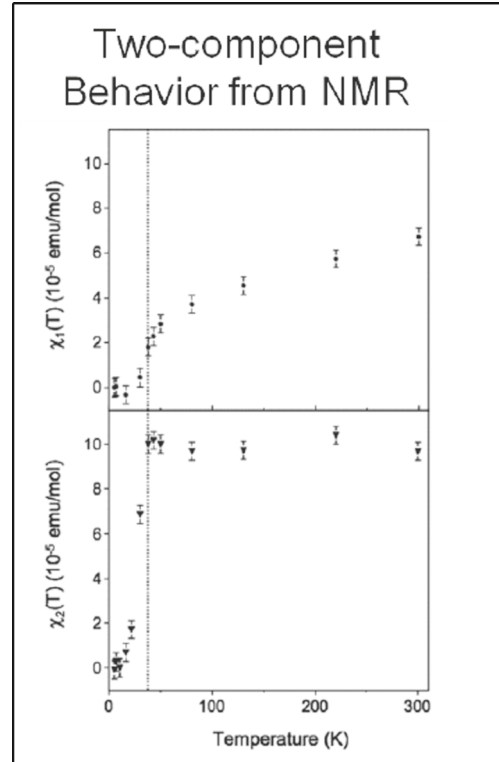
Panel 52
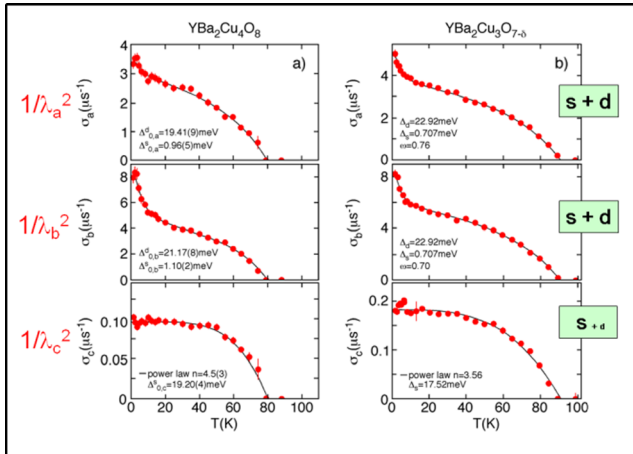
Here we show the square of the inverse of the London penetration depth for muons stopped in the bulk of LSCO along the crystallographic *a*, *b*, and *c* directions. For *a* and *b*, because of the near tetragonal crystal, they are the same, as also seen in the left figure, *but along the c-axis, it is pure s!!* This is borne out by the vibronic theory; see panels 16 and 17 (left from [1], right adapted from [49]).
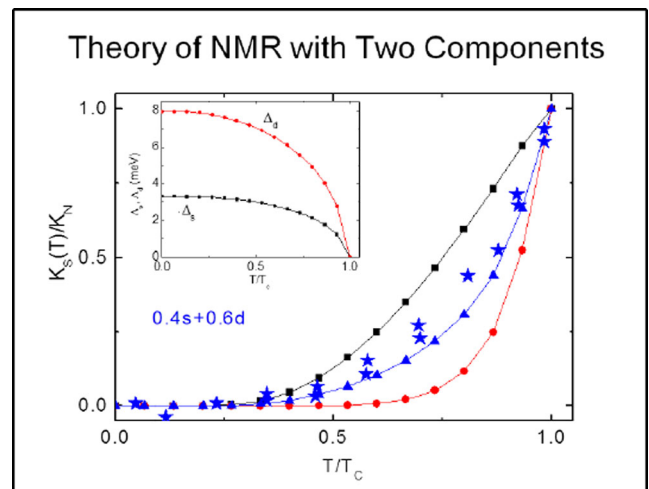
Panel 53
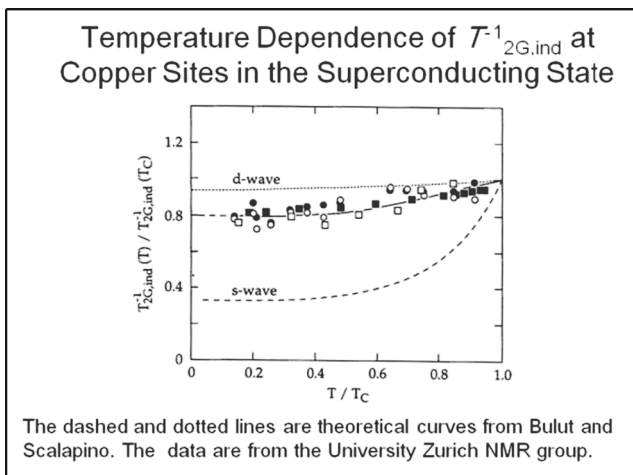
A dozen years earlier, the NMR group of the University of Zurich measured the T_{2G} relaxation of copper of LSCO [50]. As shown, the inverse of T_{2G} as a function of reduced temperature lies *in between* the quantities computed by Bulut and Scalapino [51]. Interpolating linearly between the theoretical curves in the panel, a 20 to 25 % *s* character was obtained—most remarkably in very good agreement with the muon spin rotation experiments in LSCO; see panels 51 and 52 (from [50]).

Panel 54

More recently, Haase and Slichter and their groups found clear *two-component* behavior from the susceptibility behavior as obtained by NMR (reprinted from [52]).

Panel 55

Using her vibronic theory, panels 16 and 17, Bussmann-Holder obtained 40 % *s* and 60 % *d* character from this new

data, a somewhat higher s percentage. In the inset, the s and d gaps are reproduced, all as a function of temperature (reprinted from [53]).

Panel 56

> Cuprate superconductors with unique properties have to be understood on the basis of (bi-)polaron formation and local clustering or equivalently by vibronic theory.
>
> The separation of electronic and lattice degrees of freedom, i.e., the Born–Oppenheimer approximation, has to be abandoned, also with the RVB and t-J models with purely electronic degrees of freedom.

This is the final message, which was often projected after the presentations. More on this follows in the concluding remarks.

3 Concluding Remarks

A vast number of photoemission experiments exist. Out of all of these, only the one by Lanzara et al. has been shown. The reason is twofold. In this type of experiments, the band dispersion of energy versus the wave vector is obtained, whereas the stage for the occurrence of superconducting correlations in the copper oxides is in the real space and time domain because of the polaronic character of the quasiparticles involved. This should have become obvious in the experiments discussed. Access to this phenomenon was reached via X-rays, muon spin rotation, EPR, NMR, NQR, XANES, inelastic neutron scattering, and computer simulations. In contrast, photoemission data require Fourier transformation from the energy–wave vector space into the time-dependent real space, where the essential is happening. A further difficulty is that in photoemission, the escape length of carriers is limited approximately to one lattice distance. This surface sensitivity promptly yields d wave symmetry of the superconducting wave function, predicted by the one-band theories, whereas in the CuO_2 plane in the bulk, about 25 % s component is present and relevant. The latter is due to the second band of the vibronic wave function. Along the c direction, it is *entirely s*, not observed at all by photoemission but by muon spin rotation, see panels 52 and 53(!!), as well as in optical reflectivity along the c-axis [47, and references therein, 54].

The emphasis put on experiments reflecting real space and time properties rather than on those yielding energies in the wave vector space is well supported by a recent theoretical study from the South China Normal University

in Guangzhou [55]. In it, with high accuracy, the equivalence of the observed Fermi arcs, Fermi pockets, and superstructures in cuprates by photoemission with that of a short-range diagonal stripe phase with wave vector ($7\pi/8$, $7\pi/8$) was shown. In this study, it was also pointed out that the stripe phase has nothing to do with the superconducting pairing. Incorporating a d wave pairing into the stripe phase yields the well-known gap features in the density of states.

The pairing results, in our exposition, from the presence of bipolarons (panels 31, 32, 35, and 38) and their coupling into clusters or stripes (panels 44, 45, 48, and 49). This quasiparticle description following Heisenberg is equivalent to a Schrödinger one using electronic bands and a vibronic coupling between at least the ground state and an excited band as exposed in panels 17 to 19.

In the panels shown, a relevant type of experiments has not been presented, namely Oyanagi's measurements of the fluctuations of the O–Cu distance with X-rays that show peaks at T_c and T^*. These—as well as their shapes—could be well accounted for by Bussmann-Holder et al. [56] with the presence of a substantial s wave component in the superconducting wave function, as is borne out by the muon and NMR measurements shown (panels 51 to 55). Thus, the entire data discussed are consistent with one another. There is no reason to pretend that HTS in cuprates is not understood. This is only the case if one negates the polaronic origin of the phenomenon.

References

1. Khasanov, R., Shengelaya, A., Karpinski, J., Bussmann-Holder, A., Keller, H., Müller, K.A.: J. Supercond. Novel Magn. **21**, 81 (2008)
2. Müller, K.A.: J. Phys. Condens. Matter. **19**, 251002 (2007) gives an overview
3. Weyeneth, S., Müller, K.A.: J. Supercond. Novel. Magn. **24**, 1235 (2011)
4. Bednorz, J.G., Müller, K.A.: Z. Phys. B – Cond. Matt. **64**(2), 189 (1986)
5. Bednorz, J.G., Müller, K.A.: Perovskite type oxides—the new approach to high-T_c superconductivity. Nobelprize.org. Nobel Media AB 2013. http://www.nobelprize.org/nobel_prizes/physics/laureates/1987/bednorz-lecture.html. Accessed 24 Apr 2014
6. The Kavli Foundation Special Symposium: Nobelist Perspectives on 100 Years of Superconductivity, APS March Meeting 2011, Dallas, TX (2011)
7. Symposium at the University of Twente, The Netherlands, 16 September 2011, H. Rogalla, chair
8. 3rd International Conference on Superconductivity and Magnetism (ICSM 2012), Istanbul, Turkey (2012)

9. ICAM/I2CAM Sponsored session "The foundations of high-temperature superconductivity: twenty-five years young" at the International Conference on Materials and Mechanisms of Superconductivity (M2S 2012), Washington DC (2012)

10. Chu, C.W., Gao, L., Chen, F., Huang, Z.J., Meng, R.L., Xue, Y.Y.: Nature **365**, 323 (1993)

11. Deutscher, G.: Nature **397**, 410 (1999)

12. Hüfner, S., Hossain, M.A., Damascelli, A., Sawatzky, G.A.: Rep. Prog. Phys. **71**, 062501 (2008)

13. Lanzara, A., Zhao, G.-M., Saini, N.L., Bianconi, A., Conder, K., Keller, H., Müller, K.A.: J. Phys. Condens. Matter. **11**, L541 (1999)

14. Rubio Temprano, D., Mesot, J., Janssen, S., Conder, K., Furrer, A., Mutka, H., Müller, K.A.: Phys. Rev. Lett. **84**, 1990 (2000)

15. Rubio Temprano, D., Conder, K., Furrer, A., Trouvon, V., Müller, K.A.: Phys. Rev. B **66**, 184506 (2002)

16. Müller, K.A.: Nature **377**, 133 (1995)

17. Bussmann-Holder, A., Keller, H.: Eur. Phys. J. B **44**, 487 (2005)

18. Keller, H., Bussmann-Holder, A., Müller, K.A.: Mater. Today **11**(9), 38 (2008)

19. (a) Kresin, V.Z., Wolf, S.A.: Phys. Rev. B **49**, 3652 (1994); (b) Kochelaev, B.I., Müller, K.A., Shengelaya, A.: J. Mod. Phys. **5**, 473 (2014)

20. Weyeneth, S., Müller, K.A.: J. Supercond. Novel Magn. **24**, 1235 (2011)

21. Pintchovius, L., Reichart, W.: In: Ginsberg, D.M. (Ed.) Physical Properties of High Temperature Superconductors IV, p. 295. World Scientific (1994)

22. McQueeney, R.J., Petrov, Y., Egami, T., Yethiraj, M., Shirane, G., Endoh, Y.: Phys. Rev. Lett. **82**, 628 (1999)

23. Petrov, Y., Egami, T., McQueeney, R.J., Yethiraj, M., Mook, H.A., Dogan, F.: Phonon signature of charge inhomogeneity in high temperature superconductors YBa$_2$Cu$_3$O$_{6+x}$ (2000). preprint arXiv:cond-mat/0003414v1

24. Lanzara, A., Bogdanov, P.V., Zhou, X.J., Kellar, S.A., Feng, D.L., Lu, E.D., Yoshida, T., Eisaki, H., Fujimori, A., Kishio, K., Shimoyama, J.-I., Nodak, T., Uchidak, S., Hussain, Z., Shen, Z.-X.: Nature **412**, 510 (2001)

25. Mihailovic, D., Müller, K.A.: High-T_c Superconductivity 1996: Ten Years after the Discovery, NATO ASI Series: Series E. Applied Sciences, vol. 343. Kluwer Academic, Dordrecht (1997)

26. Bianconi, A., Saini, N.L., Lanzara, A., Missori, M., Rossetti, T., Oyanagi, H., Yamaguchi, H., Oka, K., Ito, T.: Phys. Rev. Lett. **76**, 3412 (1996)

27. Müller, K.A.: In: Schrieffer, J.R., Brooks, J.S. (eds.) Handbook of High-Temperature Superconductivity, p. 1. Springer, New York (2007)

28. Emery, V.J., Reiter, G.: Phys. Rev. B **38**, 4547 (1988)

29. Kochelaev, B.I., Sichelschmidt, J., Elschner, B., Lemor, W., Loidl, A.: Phys. Rev. Lett. **79**, 4274 (1997)

30. Anderson, P.W.: Rev, Phys. Lett. **34**, 953 (1975)

31. Kabanov, V.V., Mihailovic, D.: J. Supercond.: Incorp. Novel Magn. **13**(6), 959 (2000)

32. Mihailovic, D., Kabanov, V.V.: Phys. Rev. B **63**, 054505 (2001)

33. Saini, N.L., Lanzara, A., Oyanagi, H., Yamaguchi, H., Oka, K., Ito, T., Bianconi, A.: Phys. Rev. B **55**, 12759 (1997)

34. Kochelaev, B.I., Kan, L., Elschner, B., Elschner, S. Phys. Rev. B **49**(18), 13106 (1994)

35. Shengelaya, A., Keller, H., Müller, K.A., Kochelaev, B.I., Conder, K.: J. Supercond. Incorp. Novel Magn. **13**, 955 (2000)

36. Ando, Y., Segawa, K., Komiya, S., Lavrov, A.N.: Phys. Rev. Lett. **88**, 137005 (2002)

37. Shengelaya, A., Bruun, M., Kochelaev, B.I., Safina, A., Conder, K., Müller, K.A.: Phys. Rev. Lett. **93**, 017001 (2004)

38. Alexandrov, A.S., Kabanov, V.V., Mott, N.F.: Phys. Rev. Lett. **77**, 4796 (1996)

39. Bi, X.-X., Eklund, P.C.: Phys. Rev. Lett. **70**, 2625 (1993)

40. Müller, K.A., Zhao, G.-M., Conder, K., Keller, H.: J. Phys. Condens. Matter. **10**, L291 (1998)

41. Mihailovic, D., Kabanov, V.V., Müller, K.A.: Europhys. Lett. **57**, 254 (2002)

42. Tranquada, J.M.: In: Schrieffer, J.R., Brooks, J.S. (eds.) Handbook of High-Temperature Superconductivity, p. 257. Springer, New York (2007)

43. Mertelj, T., Kabanov, V.V., Mihailovic, D.: Phys. Rev. Lett. **94**, 147003 (2005)

44. Kabanov, V.V., Mertelj, T., Mihailovic, D.: J. Supercond. Novel Magn. **19**, 67 (2006)

45. Tsuei, C.C., Kirtley, J.R.: Rev. Mod. Phys. **72**, 969 (2000)

46. Iachello, F.: Phil. Mag. Lett. **82**, 289 (2002)

47. Müller, K.A.: Applied Superconductivity 2003. In: Andreone, A., Piero Pepe, G., Cristiano, R., Masullo, G. (eds.) Proceedings of 6th European Conference on Applied Superconductivity, Sorrento, Italy, Sept. 2003, Conf. Series no. 181, pp. 3–9. IOP Publishing, London (2004)

48. Khasanov, R., Shengelaya, A., Maisuradze, A., La Mattina, F., Bussmann-Holder, A., Keller, H., Müller, K.A.: Phys. Rev. Lett. **98**, 057007 (2007)

49. Khasanov, R., Strässle, S., Di Castro, D., Masui, T., Miyasaka, S., Tajima, S., Bussmann-Holder, A., Keller, H.: Phys. Rev. Lett. **99**, 237601 (2007)

50. Stern, R., Mali, M., Roos, J., Brinkmann, D.: Phys. Rev. B **51**, 15478 (1995)

51. Bulut, N., Scalapino, D.J.: Phys. Rev. Lett. **67**, 2898 (1991)

52. Haase, J., Slichter, C.P., Williams, G.V.M.: J. Phys. Condens. Matter. **20**, 434227 (2008)

53. Bussmann-Holder, A.: J. Supercond. Novel Magn. **25**, 155 (2012)

54. Müller, K.A.: Phil. Mag. Lett. **82**, 279 (2002)

55. LiMing, W., Ke, S., Luo, J., Yin, C., Hu, L.: J. Supercond. Novel Magn. **26**, 2397 (2013)

56. Bussmann-Holder, A., Keller, H., Bishop, A.R., Simon, A., Müller, K.A.: J. Supercond. Novel Magn. **21**, 353 (2008)